Nano Energy 64 (2019) 103934

Contents lists available at ScienceDirect

Nano Energy

journal homepage: www.elsevier.com/locate/nanoen

Full paper

# 14%-efficiency fullerene-free ternary solar cell enabled by designing a short side-chain substituted small-molecule acceptor

Yuan Chang[a,b,e,1], Xin Zhang[b,c,1], Yabing Tang[d], Monika Gupta[b], Dan Su[b], Jiaen Liang[b,e], Dong Yan[b], Kun Li[b], Xuefeng Guo[c,**], Wei Ma[d,***], He Yan[e], Chuanlang Zhan[a,b,*]

[a] College of Chemistry and Environmental Science, Inner Mongolia Normal University, Huhhot, 010022, China
[b] Beijing National Laboratory for Molecular Sciences, CAS Key Laboratory of Photochemistry, Institute of Chemistry, Chinese Academy of Sciences, Beijing, 100190, China
[c] Center for Nanochemistry, Beijing National Laboratory for Molecular Sciences, State Key Laboratory for Structural Chemistry of Unstable and Stable Species, College of Chemistry and Molecular Engineering, Peking University, Beijing, 100871, China
[d] State Key Laboratory for Mechanical Behavior of Materials, Xi'an Jiaotong University, Xi'an, 710049, China
[e] Department of Chemistry and Hong Kong Branch of Chinese National Engineering Research Center for Tissue Restoration & Reconstruction, Hong Kong University of Science and Technology, Clear Water Bay, Kowloon, Hong Kong, China

ARTICLE INFO

*Keywords:*
Small-molecule acceptor
Ternary solar cell
Fullerene-free
Nonfullerene
Organic photovoltaic

ABSTRACT

A new fused-ring electron acceptor (FREA) IEICF-DMOT was designed and synthesized with 3,4-dimethoxylthiophene (DMOT) as the π − bridges to link the IDT core and the end IC-2F units. Compared to IEICO-4F which uses 3-(2-ethylhexyloxyl)thiophene as the bridge, IEICF-DMOT with two much shorter side chains (methoxyl) on the π − bridge exhibits a higher level of the lowest unoccupied molecular orbital (LUMO) (−3.85 vs. −3.93 eV), broadening absorption band, larger absorptivity, and a larger bandgap (1.38 vs. 1.27 eV), but reduced crystallinity in both the in-plane (100) and out-of-plane (010) directions, which makes a 0.13 V-larger open-circuit voltage ($V_{oc}$) with a 10%-higher external quantum efficiency (EQE) and 9%-higher fill factor (FF), and thereby, a power conversion efficiency (PCE) of 13% in comparison with the IEICO-4F 10% efficiency. Adding the crystalline and narrower bandgap IEICO-4F as the near infrared absorber, the PBDB-T:IEICF-DMOT:IEICO-4F (1:1:0.1) ternary blend shows increased crystallinity for both donor and acceptor phases with increased hole and electron mobilities, achieving increased short-circuit current-density ($J_{sc}$) and FF, and therefore, a promising PCE of 14%. These results indicate that DMOT with short side-chains on the thiophene-3,4-positions is a promise bridge unit to design nonfullerene small-molecule acceptors with tunable energy levels, optical bandgap, and crystallinity to simultaneously increase $V_{oc}$, EQE, and FF, and ultimately, efficiency.

## 1. Introduction

Polymer solar cell (PSC) that employs a blend of an electron donor polymer and an electron acceptor small-molecule has received a great attention in the past decades due to their potentials to convert the green and sustainable solar light into electric power in ways that are low-cost, light-weight, semi-transparency, and mechanical-flexibility. Breakthroughs have been recently achieved with the ITIC (3,9-bis(2-methylene-(3-(1,1-dicyanomethylene)indanone))-5,5,11,11-tetrakis(4-*n*-hexylphenyl)-dithieno[2,3d:2′,3′d′]-*s*-indaceno[1,2b:5,6b']dithiophene) [1] like fused-ring nonfullerene small molecules [2–15] and the dithionothiophen[3,2,b]-pyrrolobenzothiadiazole based acceptors [16,17] such as Y6 [18], which leads to over 14% power conversion efficiencies (PCEs) reported from binary devices recently [19,20]. These molecules are constructed in either A − D − A or A − π − D − π − A type, in which the fused-ring electron-donating (D) unit is linked with the fused-ring electron-accepting (A) units through a single carbon-carbon bond or a π − bridge. A distinct feature of the ITIC like acceptors is the perpendicular side-chains attached on the fused $sp^3$-carbon of the electron-rich core [21], such as on the 4,4,9,9-posiitons of IDTT (4,4,9,9-tetrakis(*p*-hexylphenyl)-4,9-dihydro-*s*-indaceno[1,2-b:5,6-b′] dithiophene) core, which act as steric effects to direct the acceptor molecules packing into a three-dimensional (3-D) *J* − type architecture in which the perpendicular side-chains orient in the out-of-plane (OOP)

* Corresponding author. College of Chemistry and Environmental Science, Inner Mongolia Normal University, Huhhot, 010022, China.
** Corresponding author.
*** Corresponding author.
*E-mail addresses:* guoxf@pku.edu.cn (X. Guo), msewma@mail.xjtu.edu.cn (W. Ma), clzhan@iccas.ac.cn (C. Zhan).
[1] These authors contribute equally.

https://doi.org/10.1016/j.nanoen.2019.103934
Received 13 May 2019; Received in revised form 28 June 2019; Accepted 23 July 2019
Available online 25 July 2019

direction, the same direction of the OOP oriented ππ−stacks [22], as demonstrated by the single crystal structures [23–25]. Following the pictures viewed from these single crystal structures, one can image that the side chains on the ITIC like acceptors can be divided into two classes. One is those chains perpendicular to the conjugated backbone plane. The other one is those side chains oriented within the conjugated backbone plane, such as on the 4,8-positions of the fused benzodithiophene (BDT) [26–29], on the fused N-position [30–32], on the fused thiophene/benzene of the electron-rich core [33–35], and on the π−bridges of A−π−D−π−A type molecules [36–41], as well as the chains on the ending A units [42–45]. It has been observed that the side chains on the BDT-4,8-posiitons can tune energy levels of the Frontier molecular orbitals (FMOs) due to the electron-donating nature of the side chains [46,47] and tune the electron mobility due to the modulation on morphology [48,49], and hence, the solar cell performance.

In this contribution, we report a promising new π-bridge, 3,4-dimethoxylthiophene (DMOT), with which a new FREA, named as IEICF-DMOT (2,2′-((2Z, 2′Z)-((5,5′-(4,4,9,9-tetrakis(*p*-hexylphenyl))-4,9-dihydro-*s*-indaceno[1,2-b:5,6-b′]dithiophene-2,7-diyl)bis(3-(3,4-dimethoy)thiophene-5,2-diyl))bis(methanylylidene))-bis(5,6-difluoro-3-oxo-2,3-dihydro-1H-indene-2,1-diylidene-))dimalononitrile) (Fig. 1) is synthesized and reported herein. The π-bridge mediates the electron-coupling between the D and A units and the coplanarity increase, for example, by non-covalent interactions between the bridge and the D and A units [50] helps to tune the optical, electrochemical, and photovoltaic properties of the acceptor [51]. In comparison to IEIC (2,2′-((2Z, 2′Z)-((5,5′-(4,4,9,9-tetrakis(*p*-hexylphenyl)-4,9-dihydro-*s*-indaceno[1,2-b:5,6-b′]dithiophene-2,7-diyl)bis(3-(2-ethylhexyl)thiophene-5,2-diyl))bis(methanylylidene))-bis(3-oxo-2,3-dihydro-1H-indene-2,1-diylidene))dimalononitrile) [52], the O···S non-covalent interaction [50] between the 2-ethylhexoyl O on the bridged thiophen-3-position and the fused-thiophene S of the electron-rich core in IEICO [53] helps to enhance the intramolecular charge transfer (ICT), which tunes the energy levels of FMOs. The use of a strong electron-accepting unit such as IC-2F (2-methylene-5,6-di-fluoro-3-(1,1-dicyanomethylene)indanone) yields IEICO-4F with a much narrow optical bandgap ($E_g^{opt}$). However, the highest occupied molecular orbital (HOMO) level of IEICO-4F is about −5.4 eV, and therefore, IEICO-4F can be only considered to pair with a donor polymer having a higher-HOMO-level than −5.4 eV. However, its deep lowest unoccupied molecular orbital (LUMO), about −4 eV, greatly limits the possibility to obtain a large $V_{oc}$, for example, only a value of 0.69 V has been obtained when paring with PBDTTT-E-T, though the device $J_{sc}$ reached 22.3 mA/cm$^2$ [54].

Again, compared to IEICO, the fluorination on the 5,6-positions of the fused benzene of the IC unit decreases the FWHM value (2143 vs. 2861 cm$^{-1}$). Density functional theory (DFT) calculations indicate that the 3-carbon of the bridged thiophene is involved in the HOMO, while it is a node in the LUMO. This explains the large upshift of the HOMO energy from IEIC to IEICO, while the LUMO level changes slightly. Oppositely, the 4-carbon is a node on the HOMO, but it contributes a lot to the LUMO, which greatly encourages us to substitute the thiophene 4-position with an electron-donating unit so as to raise the LUMO level, and thereby, the device $V_{oc}$. Bo et al. had reported that compared to the usage of the 3-(2-ethylhexoyl)thiophene for IEICO-4F, using 3,4-di(2-ethylhexoyl)thiophene had led to the upshifting of the LUMO level of that acceptor, therefore, obtained a much larger $V_{oc}$ (0.897 vs. 0.771 V) when pairing with the donor polymer of PBDB-T [45]. Nevertheless, the device FF was yet low, only 64%. The relatively low FF might be associated with its great crystallinity originated from the long side-chains of the π−bridge. Taken considerations of these, we turn to choose DMOT, which contains the much short methoxyl, rather than the relatively long 2-ethylhexoyl, as the side chains so as to not only raise the LUMO level but also reduce the cyrstallinity.

Our results indicate that compared to IEICO-4F, the newly synthesized IEICF-DMOT shows much broadening absorption with a larger full-width-at-the-half-maximum value (4073 vs. 2143 cm$^{-1}$), a larger absorption coefficient (2.9 vs. 2.2 × 10$^{-5}$ M$^{-1}$cm$^{-1}$), a higher LUMO energy (−3.85 vs. −3.93 eV), a larger $E_g^{opt}$ (1.39 vs. 1.29 eV), but reduced crystallinity in both the in-plane (IP) and out-of-plane (OOP) directions. When pairing with PBDB-T [55], a PCE of 13% with a $V_{oc}$ of 0.87 V, a $J_{sc}$ of 22.1 mA/cm$^2$, and an FF of 67.5% is obtained. In comparison, the IEICO-4F binary solar cell shows a PCE of 10% with a $V_{oc}$ of 0.74 V, a $J_{sc}$ of 23.1 mA/cm$^2$, and an FF of 58.4%. When using IEICO-4F as the near infrared (NIR) absorber, the resulting ternary device with a ratio of PBDB-T:IEICF-DMOT:IEICO-4F = 1:1:0.1 supplies a PCE of 14% with increased $J_{sc}$ and FF.

## 2. Results and discussion

### 2.1. Synthesis

The IEICF-DMOT was synthesized by following the procedures shown in Fig. 2. An aldehyde group was first introduced onto the commercial 3,4-dimethoythiophene 5-position in a yield of 72% with *n*-Buli and DMF as the solvent medium. The product of DMOT-CHO was then brominated on its 2-position, affording DMOT-Br-CHO in a yield of 95%. Stille coupling between IDT-2Sn and DMOT-Br-CHO yielded IDT-2DMOTCHO in a yield of 70%. The condensation between IC2F, which was synthesized by following the reported procedure [56], and IDT-2DMOTCHO afforded the desired product with a yield of 85%. The synthetic details were given in the organic synthesis part of Supporting Information.

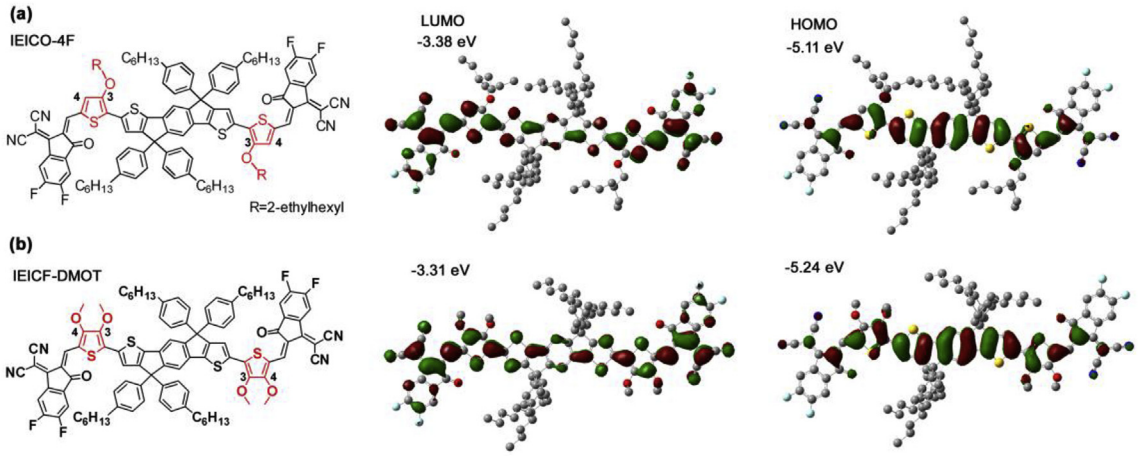


**Fig. 1.** Molecular structures and the LUMO and HOMO distributions of the acceptor molecules IEICO-4F (a) and IEICF-DMOT (b).

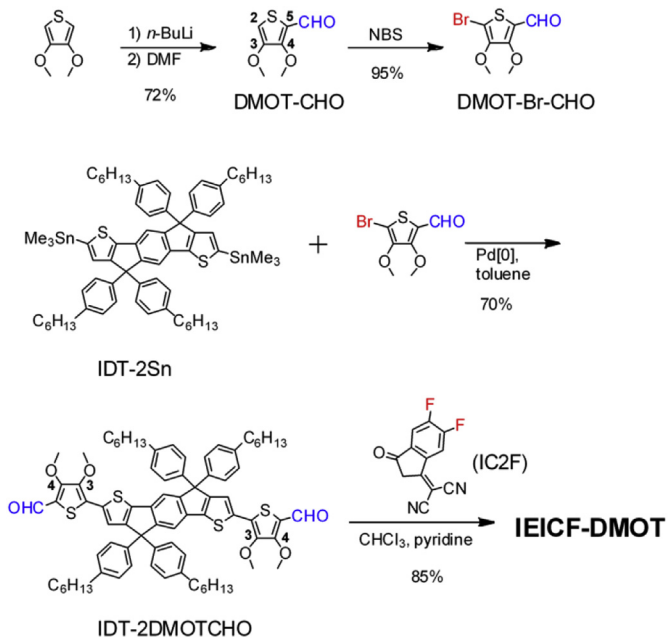


**Fig. 2.** Synthetic routes towards DMOT and IEICF-DMOT.

### 2.2. Optical and electrochemical properties

In dilute chloroform solution, IEICF-DMOT exhibits an absorption band positioning at 733 nm, which is much blue-shifted compared to that of IEICO-4F (Fig. 3a). The absorption coefficients are of 2.9 and $2.2 \times 10^{-5}\,M^{-1}cm^{-1}$, respectively, for IEICF-DMOT and IEICO-4F (Table 1). In thin film, IEICF-DMOT shows an absorption peak at 766 nm. The absorptivity is 1.64 and $0.85 \times 10^{-5}\,cm^{-1}$, respectively, for IEICF-DMOT and IEICO-4F (Table 1). The $E_g^{opt}$ value is estimated to be 1.38 eV from the absorption onset of the film (892 nm), which is increased by 0.11 eV compared to that of IEICO-4F (1.27 eV, 964 nm). The full-width-at-the-half-maximum (FWHM) values are of 2417 and $1876\,cm^{-1}$ for IEICF-DMOT and IEICO-4F estimated from their dilute chloroform solutions, respectively, and in the thin films, they are 4073 and $2143\,cm^{-1}$, respectively.

From the cyclic voltammetry (CV) data (Fig. S1), the LUMO/HOMO energy levels were determined under the same conditions to be −3.85/−5.49 eV for IEICF-DMOT and −3.93/−5.39 eV for IEICO-4F, respectively (Fig. 3b). Compared to that of IEICO-4F, the LUMO energy of IEICF-DMOT is upshifted by 0.08 eV, while the HOMO level is down shifted by 0.10 eV. DFT calculations (Fig. 1b and c) indicate that both the IEICF-DMOT and IEICO-4F molecules are highly coplanar. The dihedral angle (Table S1) between the IDT core and the bridge is 4.25° and 7.73° for IECIF-DMOT and IEICO-4F, respectively. The dihedral angle between the bridge and end IC-2F is 5.74° and 0.47° for IECIF-DMOT and IEICO-4F, respectively. The HOMO energies of IEICF-DMOT and IEICO-4F are of −5.24 and −5.11 eV, and their LUMO energies are of −3.38 and −3.31 eV, respectively. The experimental and DFT calculation data match well in the same trend. The HOMO and LUMO distributions are both similar for the two molecules. The 3-carbon of the bridged thiophene is a node of the acceptor LUMO, while the bridged thiophen-4-carbon is a node of the HOMO. Therefore, the oxygen on the bridged thiophen-3-carbon contributes to the HOMO, while no contributions to the LUMO. Oppositely, its 4-position oxygen contributes to the LUMO, but little to the acceptor HOMO.

### 2.3. Crystallinity of IEICF-DMOT and IEICO-4F

The crystallinity of the pure IEICF-DMOT and IEICO-4F films have been tested with graze-incidence wide-angle X-ray scattering (GIWAXS). The data are shown in Fig. 4. The (100) peaks are observed at about $0.30\,Å^{-1}$ in the IP direction for IEICF-DMOT and IEICO-4F, respectively. The (010) scattering peaks are seen at about 1.79 and $1.81\,Å^{-1}$ in the OOP direction, corresponding to a ππ−stacking distance of 3.51 and 3.47 Å. Compacted ππ−stacks are formed for IEICO-4F. Another distinct difference is seen in the diffraction intensity. The (010) and (100) scattering are much more intense for IEICO-4F, suggesting greater cyrstallinity which is relative to the long side chains, 2-ethylhexyloxyl, on the bridged thiophene-3-positions. Nevertheless, similar crystalline coherent length (CCL) values are estimated for both IEICO-4F and IEICF-DMOT, either in the OOP (010) or the IP (100) directions as shown in Table 1, meaning that the replacement of the 3-(2-ethylhexylthiophene) with DMOT as the bridge does not reduce the crystalline coherent size of the aggregated domains.

### 2.4. Solar cell device property

The photovoltaic property of IEICF-DMOT was investigated using a normal device structure of ITO/PEDOT:PSS [57]/PBDB-T:IEICF-DMOT/PDINO/Al. Here, PBDB-T is poly[(2,6-(4,8-bis(5-(2-ethylhexyl)thiophen-2-yl)benzo[1,2-*b*:4,5-*b′*]dithiophene)-*co*-(1,3-di(5-thiophene-2-yl)-5,7-bis(2-ethylhexyl)benzo[1,2-*c*:4,5-*c′*]dithiophene-4,8-dione) [58] and PDINO is amino N-oxide perylene diimide [59]. The weight ratio of PBDB-T:IEICF-DMOT was 1:1 and a thermal annealing process at 100 °C for 10 min was applied to the active layer. 1% DIO (1,8-diiodooctane) was used for optimizing the IEICO-4F binary devices. No slvent additives were used for the optimizations of the IEICF-DMOT based binary and ternary solar cells. The optimizations were shown in Table S2.

Fig. 5a displays the current-density − voltage ($J-V$) curves from the optimal cells. The $V_{oc}$ and $J_{sc}$ and *FF* of the PBDB-T:IEICF-DMOT device are of 0.870 V, 22.14 mA/cm$^2$ and 0.675, which ultimately afford a PCE of 13.01% (Table 2). The energy loss $E_{loss}$ is estimated to be 0.51 eV by following Eq. $E_{loss} = E_g^{opt} - eV_{oc}$. Compared to the PBDB-T:IEICO-4F cell, the $V_{oc}$ from IEICF-DMOT based device is improved by 0.13 V, the *FF* is increased by 9%. The larger $V_{oc}$ provides a larger internal field, which contributes to the obtaining of the higher device FF. Due to the larger bandgap of IEICF-DMOT, the PBDB-T:IEICF-DMOT

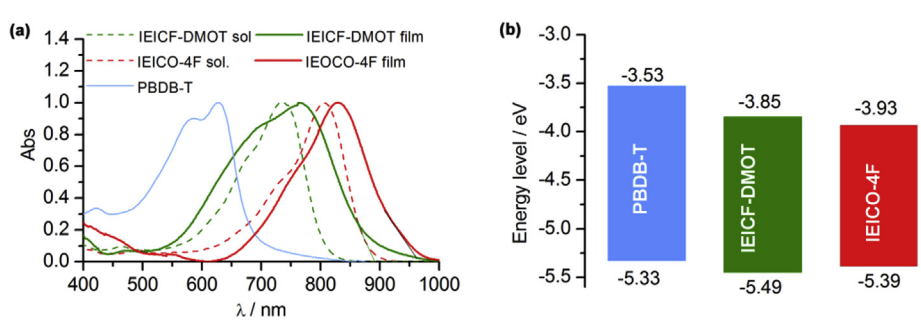


**Fig. 3.** (a) The absorption spectra of the polymer PBDB-T in thin film (solid line) and acceptors IEICF-DMOT and IEICO-4F in solution (chloroform, dash lines) and in pure thin films (solid lines). (b) The diagram of energy levels of the polymer and acceptors.

**Table 1**
Optical and electrochemical properties of the acceptor IEICF-DMOT along with the CCL values.

| | $\varepsilon_{max}$ [$10^5$ $M^{-1}cm^{-1}$] | $\lambda_{max}^{film}$ [nm] | | FWHM [$cm^{-1}$] | | Absorptivity [$10^5$ $cm^{-1}$] | $E_g^{opt}$ [eV] | LUMO [eV] | HOMO [eV] | CCL [nm] | |
|---|---|---|---|---|---|---|---|---|---|---|---|
| | | Sol. | Film | Sol. | film | film | | | | OOP | IP |
| IEICF-DMOT | 2.9 | 733 | 765 | 2417 | 4073 | 1.64 | 1.38 | −3.85 | −5.49 | 4.9 | 24.6 |
| IEICO-4F | 2.2 | 806 | 832 | 1876 | 2143 | 0.85 | 1.27 | −3.93 | −5.39 | 5.6 | 23.6 |

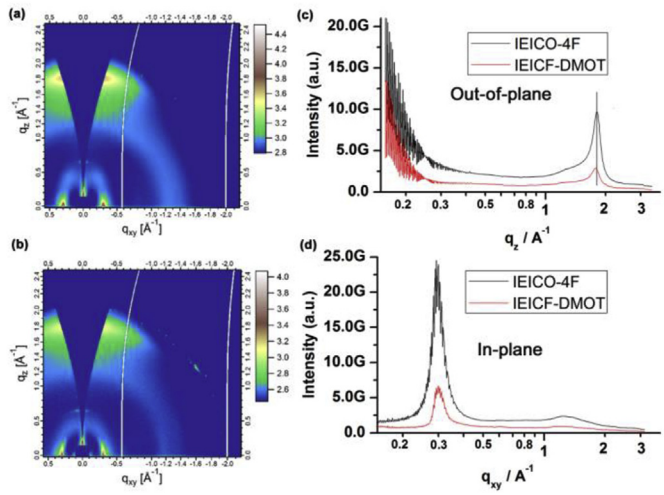


**Fig. 4.** The GIWAXS data of the pure IEICO-4F (a) and IEICF-DMOT (b) films and the line-cut profiles in the out-of-plane (c) and in-plane (d) directions, respectively.

blend covers a narrower wavelength region of the solar spectrum, 300–890 nm, in comparison to the 300–960 nm coverage for the IEICO-4F blend. However, thanks to the higher external quantum efficiency (EQE) responded in the wavelength region of 450–800 nm (Fig. 5b), larger $J_{sc}$ value is still obtained: 21.5 mA/cm$^2$ for the IEICF-DMOT and 22.2 mA/cm$^2$ for the IEICO-4F device.

IEICF-DMOT and IEICO-4F are of structural similarity and IEICO-4F shows a narrower optical bandgap, which encourages us to use IEICO-4F as a NIR absorber. We then fabricated the ternary devices with IEICO-4F as the second acceptor component. The photovoltaic properties of the ternary devices with the IEICO-4F contents varying from 0.05 to 0.3 are given in Table S3. The best device was obtained when using 0.1 IEICO-4F as the third component, which showed a PCE of 14% with increased $J_{sc}$ and *FF* and a close $V_{oc}$ compared to the IECIF-DMOT binary. The stability of the ternary device was tested under the continuous illunimation of an AM 1.5G light source and shown in Fig. S2. In the beginning of the initial 5 h, the PCE is decreased down to 12.04% (86% of the initial PCE value). Then, the PCE is gradually decreased to 5.88%. The $J-V$ curve of the best ternary device is given in Fig. 5a and b gives the EQE spectra of the ternary devices. The involvement of the 850–950 nm EQE originated from the incorporation of IEICO-4F and the increase of the 500–650 nm EQE both contribute the increase of the $J_{sc}$. The $J_{sc}$ values obtained from integrating the EQE spectra match well with those values from the $J-V$ measurements (Table 2).

### 2.5. Charge mobilities

The hole and electron mobilities ($\mu_h$ and $\mu_e$) of the binary and ternary solar cell blends were measured with space-charge-limited current (SCLC) method. The data were given in Fig. S3. Both the $\mu_h$ and $\mu_e$ values of the IEICO-4F based binary blend are higher than the IEICF-DMOT based (8.39 vs. $3.72 \times 10^{-4}$ $cm^2V^{-1}s^{-1}$ for $\mu_h$ and 4.32 vs. $1.93 \times 10^{-4}$ $cm^2V^{-1}s^{-1}$ for $\mu_e$). Upon addition of 0.1 IEICO-4F resulting a ternary ratio of PBDB-T:IEICF-DMOT:IEICO-4F = 1:1:0.1, the $\mu_h$ and $\mu_e$ value are 5.33 vs. $3.18 \times 10^{-4}$ $cm^2V^{-1}s^{-1}$, respectively, which is increased either for the hole or the electron mobility in comparisons to that of the IEICF-DMOT based binary. The increase in both the electron and hole mobilities upon addition of 0.1 IEICO-4F into the 1:1 blended PBDB-T:IEICF-DMOT film is a factor of the increased EQE of the ternary in comparison to that of the IEICF-DMOT binary device.

### 2.6. Recombination losses and collection of mobile charges

The recombination mechanisms of the mobile charges can be reflected by studying the light-dependent $J-V$ characteristics of the solar cell [60]. By plotting the $J_{sc}$ and $V_{oc}$ as a function of light intensity (Figs. S4a and b) in a power law equation $J_{sc} \propto P^{\alpha}$ and the Eq. $V_{oc} \propto n(kT/q)\ln(P)$, where k, T, and q are the Boltzmann constant, temperature in Kelvin, and the elementary charge, respectively, a $\alpha$ and $n$ value are fitted. The $\alpha$ or $n$ value approaches 1.0, indicating the recombination is dominated by the monomolecular or bimolecular mechanism at shorcircuit or open-circuit, while if it deviates from 1.0, it means the involvement of bimolecular or monomolecular recombination. The fitting $\alpha/n$ values are 0.99/1.09KT/$q$, 0.99/1.11KT/$q$ and 0.98/1.08KT/$q$ for the IEICF-DMOT and IEICO-4F based binary and their ternary devices, respectively, demonstrating that the addition of 0.1 IEICO-4F does not enhance the charge recombination. The $\alpha$ value is close to 1, suggesting the monomolecular recombination is dominated at short-circuit with weak bimolecular loss involved. The $n$ value is about 1.1, meaning the involvements of monomolecular mechanism at open-circuit.

The charge collection efficiency is reflected by the plot of photogenerated current-density ($J_{ph}$) vs. the effective voltage ($V_{eff}$) (Fig. S4c) [61] with $V_{eff} = V_{BI} - V_{bias}$, where $V_{BI}$ is the voltage when $J_{ph} = 0$ mA cm$^{-2}$, and $V_{bias}$ is the applied voltage; $J_{ph} = J_D - J_L$, where

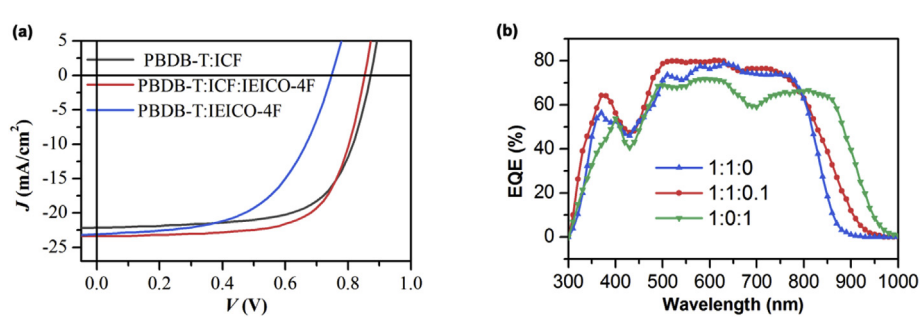


**Fig. 5.** The $J-V$ curves (a) and the EQE spectra (b) of the optimal solar cells.

**Table 2**
The photovoltaic data of the binary and ternary solar cells. All data were obtained under illumination of the AM 1.5G (100 mW/cm$^2$) light source.

| PBDB-T:IEICF-DMOT:IEICO-4F | $V_{oc}$[a] [V] | $J_{sc}$[a] [mA/cm$^2$] | $J_{sc}$[b] [mA/cm$^2$] | *FF*[a] [%] | *PCE*[a] [%] | $CCL_{OOP}$ [nm] SMA[c] | $CCL_{OOP}$ [nm] polymer[d] | $CCL_{IP}$ [nm] SMA[e] |
|---|---|---|---|---|---|---|---|---|
| 1:1:0 | 0.87 (0.87 ± 0.01) | 22.14 (21.98 ± 0.23) | 21.47 | 67.53 (66.62 ± 1.17) | 13.01 (12.79 ± 0.15) | 3.6 | 6.9 | 26.2 |
| 1:1:0.1 | 0.86 (0.86 ± 0.01) | 23.31 (23.10 ± 0.24) | 22.39 | 69.75 (69.09 ± 1.38) | 14.00 (13.73 ± 0.19) | 4.0 | 10.9 | 32.4 |
| 1:0:1 | 0.74 (0.74 ± 0.01) | 23.10 (22.87 ± 0.16) | 22.18 | 58.36 (57.29 ± 1.81) | 9.98 (9.81 ± 0.26) | 6.7 | 16.2 | 36.0 |

[a] The average value of the device parameter are calculated from 20 devices.
[b] Integrated from the EQE spectra.
[c] Calculated form the (010) scattering peak around 1.8 Å$^{-1}$ at the OOP direction (Fig. 6).
[d] Calculated form the (100) scattering peak around 0.29 Å$^{-1}$ at the OOP direction (Fig. 6).
[e] Calculated form the (100) scattering peak around 0.30 Å$^{-1}$ at the IP direction (Fig. 6).

$J_L$ and $J_D$ are the current densities under illumination and dark conditions, respectively. As the $V_{eff}$ is higher than 2 V, the $J_{ph}$ approaches to a saturated value, resulting in $J_{ph,sat}$ = 23.3 and 24.1 mA/cm$^2$ for the IEICF-DMOT and IEICO-4F based binary solar cells, respectively. The larger $J_{ph,sat}$ value is due to the more narrowed optical bandgap of IEICO-4F. The charge collection efficiency at short-circuit current is calculated by following $p_c = J_{ph,sc}/J_{ph,sat}$ to be 0.95 and 0.96, respectively. For the ternary device, the $J_{ph,sat}$ and $p_c$ are 24.0 mA/cm$^2$ and 0.97, respectively, which are both increased compared to the IEICF-DMOT binary device due to the incorporation of the narrowed IEICO-4F as the NIR absorber and agrees with the increased device FF.

### 2.7. Film-morphologies

The GIWAXS data of the binary and ternary blends are given in Fig. 6 and Fig. S5. For the IEICO-4F binary blend, a set of strong diffractions seen at q 0.311, 0.476, 1.787 Å$^{-1}$ at the OOP direction and the strong peak at 0.332 Å$^{-1}$ at the IP direction both indicate formation of great crystallinity for IEICO-4F, which can be due to the use of 1% 1,8-diiodooctane (DIO) as the solvent additive. For the IEICO-4F pure film, no solvent additives are used. The crystallnity is greatly reduced and no detailed scattering rings or arcs observed between q ~0.4–1.4 Å$^{-1}$ region. Again, for the IEICO-4F ternary blend, no solvent additives are used and no scattering peaks are seen between the q ~0.4–1.4 Å$^{-1}$ region. For the IEICF-DMOT binary blend, no solvent additives were used.

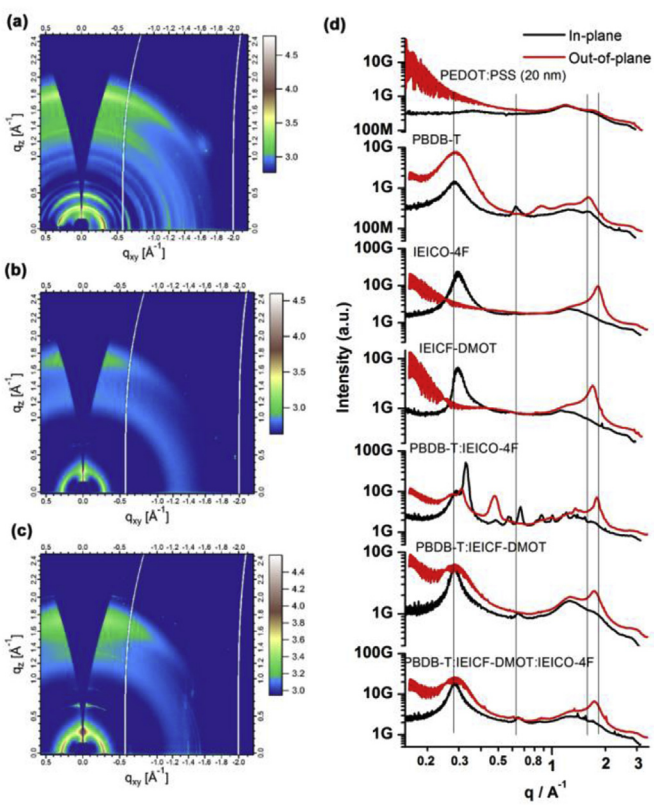


**Fig. 6.** The GIWAXS data of the IEICO-4F (a) and IEICF-DMOT (b) based binary blends and their ternary blend (c) with a ratio of PBDB-T:IEICF-DMOT:IEICO-4F = 1:1:0.1 and the line-cut profiles (d) in the out-of-plane and in-plane directions, respectively. The linecut profiles of the pure PBDB-T, IEICO-4F, and IEICF-DMOT films involved for comparisons.

We have observed that the IP (100) scattering peak can reflect the packing ordering and crystallinity of the acceptor molecules along the OOP direction, e.g. on the ππ−stacking direction [62]. In these cases, the crystallinity of the acceptor phases can be revealed by the coherent crystalline length (CCL) value calculated from the IP (100) scattering around 0.30 Å$^{-1}$, and again, by the OOP (010) scattering around 1.8 Å$^{-1}$, e.g. the ππ−stacks. The CCL values shown in Table 2 demonstrate the increase of the crystallinity of the acceptor phases upon addition of 0.1 IEICO-4F into the PBDB-T:IEICF-DMOT (1:1) blend. Again, the PBDB-T phase crystallinity is indicated by the OOP (100) scattering around 0.29Å$^{-1}$, which is increased upon the addition of IEICO-4F. The trend in the crystallinity going from the IEICF-DMOT blend to the ternary and then the IEICO-4F binary blend is in accordance with the increase of their electron and hole mobilities. Again, the increase in the acceptor phase crystallinity and no additional scattering peaks observed when IEICO-4F is added into the IEICF-DMOT binary blend suggest the mixing of the two acceptors, which is due to the similarity of the molecular structures of the two acceptors.

The morphology of the binary and ternary blends is further characterized with the resonant soft X-ray scattering (RSoXS) at 285.2 eV photon energy. The data were plotted in Iq$^2$ versus q format and given in Fig. 7. A strong and broad scattering band peaking around 0.066 Å$^{-1}$ with a hump at ~0.020 Å$^{-1}$ is observed from the IEICO-4F binary blend, suggesting the formation of multi-length scaled crystalline phase separation. The domain size is calculated to be 47.7 nm. Comparatively, a relatively weak but fine scattering band at 0.098 Å$^{-1}$ is seen in the IEICF-DMOT binary blend, which corresponds to a smaller domain size, 32.3 nm. The differences in the scattering from the RSoXS experiments further support the distinct changes in the film-morphology upon the replacement of side chains on the thiophene bridge, going from the long 2-ethylhexoyl to the short methoxyl ones. For the ternary blend with the addition of 0.1 IEICO-4F into the 1:1 blended PBDB-T:IEICF-DMOT binary, a fine scattering band yet observed implies the formation of homogeneous phase separation. The small shift from the IEICF-DMOT binary 0.098 Å$^{-1}$ to the ternary 0.090 Å$^{-1}$ relates to a small increase in the domain size (32.2 vs. 35.0 nm) and the slight increase of the scattering intensity agrees with the small increase in the phase crystallinity, as revealed by the GIWAXS data. Again, the phase purity is slightly increased from 0.62 to 0.64 after the addition of 0.1 IEICO-4F, which is consistent with the maintaining of the device FF.

Fig. 8a–c collects the transmission electron microscopy (TEM) images of the binary and ternary blends. All these three blends show

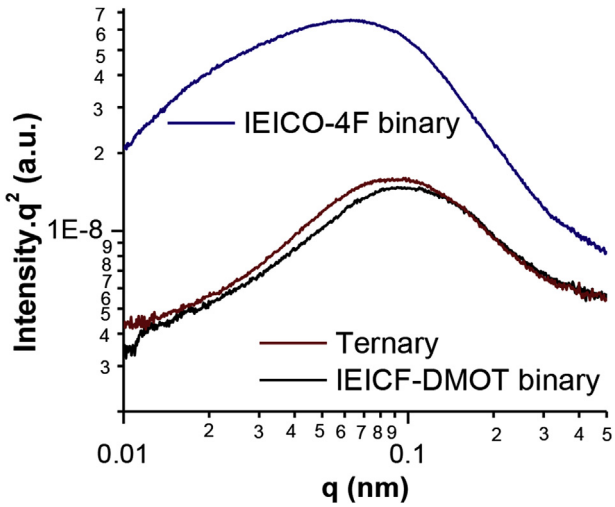


**Fig. 7.** The RSoXS data of the IEICO-4F and IEICF-DMOT based binary blends and their ternary blend with a ratio of PBDB-T:IEICF-DMOT:IEICO-4F = 1:1:0.1.

nanoscaled phase-separated bright and dark domains. The thinner morphology observed on the IEICF-DMOT in comparison to the crystalline fibril morphology seen on the IEICO-4F blend is consistent with the morphology revealed by the GIWAXS and RSoXS data and agrees with the higher FF of the IEICF-DMOT binary device. Upon addition of IEICO-4F into the PBDB-T:IEICF-DMOT blend, fine and homogenous morphology is observed, which again suggests the mixing of the two acceptors and agrees with the high FF of the ternary solar cell. Fig. 8d–f is the atomic force microscopy (AFM) height images. The AFM reflected surface morphology is very close to that observed from TEM. Fine morphology is seen in the IEICF-DMOT binary and the ternary blend, while fiber-like morphology is observed in the IEICO-4F blend. The room-mean-roughness (rms) value is 2.28 nm, 2.64 nm, and 3.53 nm for the IEICF-DMOT binary, the ternary, and the IEICO-4F binary blend, respectively.

From the TEM images, clear fibril morphology can be seen in the IEICF-DMOT and IEICO-4F binary and their ternary blends. The anisotropic orientation of the fibril structures will induce polarization scattering, which can be clearly seen on their 2D scattering images (Fig. 9a–c). The Iq$^2$ versus q plots (Fig. 9d–f) clearly indicate the different integrated sectors with orthogonal angles in the 2D scattering images. Compared to IEICO-4F binary blend, greater difference is seen on the IEICF-DMOT binary blend. The difference is slightly reduced with the addition of 0.1 IEICO-4F into the PBDB-T:IEICF-DMOT binary blend.

## 3. Conclusions

In summary, we have reported that 3,4-dimethoxylthiophene (DMOT) substituted by the methoxyl short side-chains is a promising π-bridge with which the synthesized small-molecule acceptor like IEICF-DMOT shows reduced crystallinity in both the out-of-plane and in-plane directions and simultaneously has a higher LUMO energy level and improved absorption of solar photons. When pairing with the donor polymer of PBDB-T, simultaneous increased $V_{oc}$, FF, and EQE are readily obtained, in comparisons to the long-side-chain 3-(2-ethylhexyloxyl)thiophene bridged acceptor such as the known IEICO-4F, and therefore a higher efficiency (13% vs. 10%) is readily obtained. The ternary device by adding 0.1 of the crystalline IEICO-4F into the PBDB-T:IEICF-DMOT binary blend displays an efficiency of 14% with increased crystallinity and higher electron and hole mobilities, compared to the host binary solar cell.

## Acknowledgments

The authors gratefully acknowledge the financial support of the National Natural Science Foundation of China (NSFC, Nos. 91433202, 21773262, 21504066, 21534003, 21327805, 21521062 and 91227112), Chinese Academy of Sciences (CAS, XDB12010200), and Ministry of Science and Technology of the People's Republic of China (No. 2016YFA0200700). X-ray data was acquired at beamlines 7.3.3 at the Advanced Light Source, which is supported by the Director, Office of Science, Office of Basic Energy Sciences, of the U.S. Department of Energy under Contract No. DE-AC02-05CH11231. The authors thank Chenhui Zhu at beamline 7.3.3 for assistance with data acquisition.

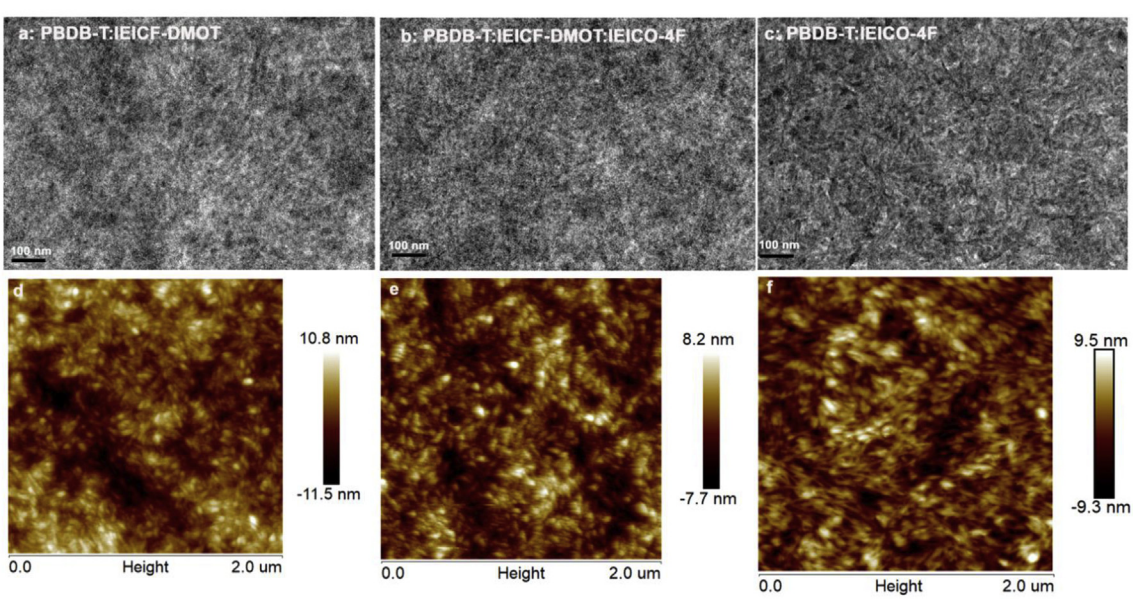


**Fig. 8.** TEM (a, b and c) and AFM height (d, e and f) pictures of the IEICF-DMOT binary (a and d), the ternary (b and e), and the IEICO-4F binary (c and f) solar cell blends, respectively.

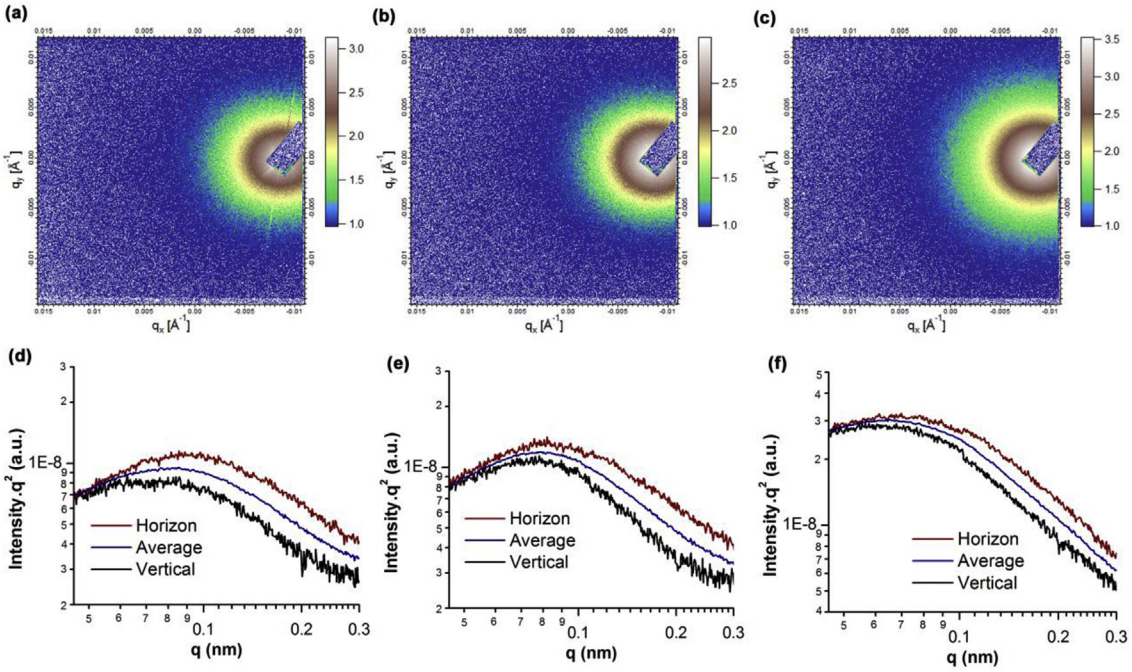


**Fig. 9.** (a, b and c) The polarization scattering 2D images and (d, e and f) the $Iq^2$ versus q plots at the vertical and horizon direction as well as the average sectors around the 360 angle for the IEICF-DMOT binary (a and d), the ternary (b and e), and the IEICO-4F binary (c and f) solar cell blends, respectively.

## Appendix A. Supplementary data

Supplementary data to this article can be found online at https://doi.org/10.1016/j.nanoen.2019.103934.

## References


[1] Y. Lin, J. Wang, Z.-G. Zhang, H. Bai, Y. Li, D. Zhu, X. Zhan, Adv. Mater. 27 (2015) 1170–1174.
[2] Y. Li, D. Qian, L. Zhong, J.-D. Lin, Z.-Q. Jiang, Z.-G. Zhang, Z. Zhang, Y. Li, L.-S. Liao, F. Zhang, Nano Energy 27 (2016) 430–438.
[3] Q. Fan, Q. Zhu, Z. Xu, W. Su, J. Chen, J. Wu, X. Guo, W. Ma, M. Zhang, Y. Li, Nano Energy 48 (2018) 413–420.
[4] W. Gao, M. Zhang, T. Liu, R. Ming, Q. An, K. Wu, D. Xie, Z. Luo, C. Zhong, F. Liu, F. Zhang, H. Yan, C. Yang, Adv. Mater. (2018) e1800052.
[5] W. Liu, J. Zhang, Z. Zhou, D. Zhang, Y. Zhang, S. Xu, X. Zhu, Adv. Mater. (2018) e1800403.
[6] Z. Yao, X. Liao, K. Gao, F. Lin, X. Xu, X. Shi, L. Zuo, F. Liu, Y. Chen, A.K.Y. Jen, J. Am. Chem. Soc. 140 (2018) 2054–2057.
[7] B. Kan, H. Feng, X. Wan, F. Liu, X. Ke, Y. Wang, Y. Wang, H. Zhang, C. Li, J. Hou, Y. Chen, J. Am. Chem. Soc. 139 (2017) 4929–4934.
[8] J. Wang, J. Zhang, Y. Xiao, T. Xiao, R. Zhu, C. Yan, Y. Fu, G. Lu, X. Lu, S.R. Marder, X. Zhan, J. Am. Chem. Soc. 140 (2018) 9140–9147.
[9] Z. Fei, F.D. Eisner, X. Jiao, M. Azzouzi, J.A. Rohr, Y. Han, M. Shahid, A.S.R. Chesman, C.D. Easton, C.R. McNeill, T.D. Anthopoulos, J. Nelson, M. Heeney, Adv. Mater. 30 (2018) 1705209.
[10] L. Zhang, B. Lin, Z. Ke, J. Chen, W. Li, M. Zhang, W. Ma, Nano Energy 41 (2017) 609–617.
[11] J. Sun, X. Ma, Z. Zhang, J. Yu, J. Zhou, X. Yin, L. Yang, R. Geng, R. Zhu, F. Zhang, W. Tang, Adv. Mater. 30 (2018) e1707150.
[12] D. Baran, R.S. Ashraf, D.A. Hanifi, M. Abdelsamie, N. Gasparini, J.A. Rohr, S. Holliday, A. Wadsworth, S. Lockett, M. Neophytou, C.J.M. Emmott, J. Nelson, C.J. Brabec, A. Amassian, A. Salleo, T. Kirchartz, J.R. Durrant, I. McCulloch, Nat. Mater. 16 (2017) 363–370.
[13] X. Li, F. Pan, C. Sun, M. Zhang, Z. Wang, J. Du, J. Wang, M. Xiao, L. Xue, Z.-G. Zhang, C. Zhang, F. Liu, Y. Li, Nat. Commun. 10 (2019) 519.
[14] Y. Zhou, M. Li, J. Song, Y. Liu, J. Zhang, L. Yang, Z. Zhang, Z. Bo, H. Wang, Nano Energy 45 (2018) 10–20.
[15] Q. Fan, Z. Xu, X. Guo, X. Meng, W. Li, W. Su, X. Ou, W. Ma, M. Zhang, Y. Li, Nano Energy 40 (2017) 20–26.
[16] J. Yuan, Y. Zhang, L. Zhou, C. Zhang, T.-K. Lau, G. Zhang, X. Lu, H.-L. Yip, S.K. So, S. Beaupre, M. Mainville, P.A. Johnson, M. Leclerc, H. Chen, H. Peng, Y. Li, Y. Zou, Adv. Mater. (2019) e1807577.
[17] J. Yuan, T. Huang, P. Cheng, Y. Zou, H. Zhang, J.L. Yang, S.-Y. Chang, Z. Zhang, W. Huang, R. Wang, D. Meng, F. Gao, Y. Yang, Nat. Commun. 10 (2019) 570.
[18] J. Yuan, Y. Zhang, L. Zhou, G. Zhang, H.-L. Yip, T.-K. Lau, X. Lu, C. Zhu, H. Peng, P.A. Johnson, M. Leclerc, Y. Cao, J. Ulanski, Y. Li, Y. Zou, Joule 3 (2019) 1–12.
[19] Z. Zheng, Q. Hu, S. Zhang, D. Zhang, J. Wang, S. Xie, R. Wang, Y. Qin, W. Li, L. Hong, N. Liang, F. Liu, Y. Zhang, Z. Wei, Z. Tang, T.P. Russell, J. Hou, H. Zhou, Adv. Mater. 30 (2018) e1801801.
[20] S. Li, L. Ye, W. Zhao, H. Yan, B. Yang, D. Liu, W. Li, H. Ade, J. Hou, J. Am. Chem. Soc. 140 (2018) 7159–7167.
[21] F. Shen, J. Xu, X. Li, C. Zhan, J. Mater. Chem. A 6 (2018) 15433–15455.
[22] D. Yan, W. Liu, J. Yao, C. Zhan, Adv. Energy Mater. 8 (2018) 1800204.
[23] G. Han, Y. Guo, X. Song, Y. Wang, Y. Yi, J. Mater. Chem. C 5 (2017) 4852–4857.
[24] X. Shi, X. Liao, K. Gao, L. Zuo, J. Chen, J. Zhao, F. Liu, Y. Chen, A.K.-Y. Jen, Adv. Funct. Mater. 28 (2018) 1802324.
[25] J. Qu, Q. Zhao, J. Zhou, H. Lai, T. Liu, D. Li, W. Chen, Z. Xie, F. He, Chem. Mater. 31 (2019) 1664–1671.
[26] Q. Liu, Z. Xiao, T. Li, S. Yang, W. You, M. Wang, L. Ding, Mater. Chem. Front. 2 (2018) 1563–1567.
[27] Z. Zhang, X. Zhu, J. Mater. Chem. A 6 (2018) 4266–4270.
[28] Y. Li, L. Zhong, B. Gautam, H.-J. Bin, J.-D. Lin, F.-P. Wu, Z. Zhang, Z.-Q. Jiang, Z.-G. Zhang, K. Gundogdu, Y. Li, L.-S. Liao, Energy Environ. Sci. 10 (2017) 1610–1620.
[29] D. Liu, L. Yang, Y. Wu, X. Wang, Y. Zeng, G. Han, H. Yao, S. Li, S. Zhang, Y. Zhang, Y. Yi, C. He, W. Ma, J. Hou, Chem. Mater. 30 (2018) 619–628.
[30] K. Wang, Y. Firdaus, M. Babics, F. Cruciani, Q. Saleem, A. El Labban, M.A. Alamoudi, T. Marszalek, W. Pisula, F. Laquai, P.M. Beaujuge, Chem. Mater. 28 (2016) 2200–2208.
[31] Y.-T. Hsiao, C.-H. Li, S.-L. Chang, S. Heo, K. Tajima, Y.-J. Cheng, C.-S. Hsu, ACS Appl. Mater. Interfaces 9 (2017) 42035–42042.
[32] C. Huang, X. Liao, K. Gao, L. Zuo, F. Lin, X. Shi, C.-Z. Li, H. Liu, X. Li, F. Liu, Y. Chen, H. Chen, A.K.Y. Jen, Chem. Mater. 30 (2018) 5429–5434.
[33] W. Wang, B. Zhao, Z. Cong, Y. Xie, H. Wu, Q. Liang, S. Liu, F. Liu, C. Gao, H. Wu, Y. Cao, Acs Energy Lett 3 (2018) 1499.
[34] D. Liu, B. Kan, X. Ke, N. Zheng, Z. Xie, D. Lu, Y. Liu, Adv. Energy Mater. 8 (2018) 1801618.
[35] F.-Y. Cao, W.-C. Huang, S.-L. Chang, Y.-J. Cheng, Chem. Mater. 30 (2018) 4968–4977.
[36] F. Liu, Z. Zhou, C. Zhang, J. Zhang, Q. Hu, T. Vergote, F. Liu, T.P. Russell, X. Zhu, Adv. Mater. 29 (2017) 1606574.
[37] F.-X. Chen, J.-Q. Xu, Z.-X. Liu, M. Chen, R. Xia, Y. Yang, T.-K. Lau, Y. Zhang, X. Lu, H.-L. Yip, A.K.Y. Jen, H. Chen, C.-Z. Li, Adv. Mater. 30 (2018) 1803769.
[38] J. Lee, S.-J. Ko, M. Seifrid, H. Lee, B.R. Luginbuhl, A. Karki, M. Ford, K. Rosenthal, K. Cho, T.-Q. Nguyen, G.C. Bazan, Adv. Energy Mater. 8 (2018) 1801212.
[39] A. Tang, B. Xiao, Y. Wang, F. Gao, K. Tajima, H. Bin, Z.-G. Zhang, Y. Li, Z. Wei, E. Zhou, Adv. Funct. Mater. 28 (2018) 1704507.
[40] S. Chen, H. Yao, B. Hu, G. Zhang, L. Arunagiri, L.-K. Ma, J. Huang, J. Zhang, Z. Zhu, F. Bai, W. Ma, H. Yan, Adv. Energy Mater. 8 (2018) 1800529.
[41] Z. Zhang, X. Zhu, Chem. Mater. 30 (2018) 587–591.
[42] B. Xiao, A. Tang, Q. Zhang, G. Li, X. Wang, E. Zhou, ACS Appl. Mater. Interfaces 10 (2018) 34427–34434.
[43] Y. Yang, J. Wang, H. Xu, X. Zhan, X. Chen, ACS Appl. Mater. Interfaces 10 (2018) 18984–18992.
[44] Suman, V. Gupta, A. Bagui, S.P. Singh, Adv. Funct. Mater. 27 (2017) 1603820.

[45] Y. Ma, M. Zhang, Y. Tang, W. Ma, Q. Zheng, Chem. Mater. 29 (2017) 9775–9785.
[46] Q. An, W. Gao, F. Zhang, J. Wang, M. Zhang, K. Wu, X. Ma, Z. Hu, C. Jiao, C. Yang, J. Mater. Chem. A 6 (2018) 2468–2475.
[47] B. Kan, J. Zhang, F. Liu, X. Wan, C. Li, X. Ke, Y. Wang, H. Feng, Y. Zhang, G. Long, R.H. Friend, A.A. Bakulin, Y. Chen, Adv. Mater. 30 (2018) 1704904.
[48] J. Wang, W. Wang, X. Wang, Y. Wu, Q. Zhang, C. Yan, W. Ma, W. You, X. Zhan, Adv. Mater. 29 (2017) 1702125.
[49] T.J. Aldrich, S.M. Swick, F.S. Melkonyan, T.J. Marks, Chem. Mater. 29 (2017) 10294–10298.
[50] J. Huang, Y. Zhao, W. He, H. Jia, Z. Lu, B. Jiang, C. Zhan, Q. Pei, Y. Liu, J. Yao, Polym. Chem. 3 (2012) 2832–2841.
[51] Y. Liu, Z. Zhang, S. Feng, M. Li, L. Wu, R. Hou, X. Xu, X. Chen, Z. Bo, J. Am. Chem. Soc. 139 (2017) 3356–3359.
[52] Y. Lin, Z.-G. Zhang, H. Bai, J. Wang, Y. Yao, Y. Li, D. Zhu, X. Zhan, Energy Environ. Sci. 8 (2015) 610–616.
[53] H. Yao, Y. Chen, Y. Qin, R. Yu, Y. Cui, B. Yang, S. Li, K. Zhang, J. Hou, Adv. Mater. 28 (2016) 8283–8287.
[54] H. Yao, Y. Cui, R. Yu, B. Gao, H. Zhang, J. Hou, Angew. Chem. Int. Ed. 56 (2017) 3045–3049.
[55] Y. Liu, C.e. Zhang, D. Hao, Z. Zhang, L. Wu, M. Li, S. Feng, X. Xu, F. Liu, X. Chen, Z. Bo, Chem. Mater. 30 (2018) 4307–4312.
[56] S. Dai, F. Zhao, Q. Zhang, T.-K. Lau, T. Li, K. Liu, Q. Ling, C. Wang, X. Lu, W. You, X. Zhan, J. Am. Chem. Soc. 139 (2017) 1336–1343.
[57] W. Li, X. Zhang, X. Zhang, J. Yao, C. Zhan, ACS Appl. Mater. Interfaces 9 (2017) 1446–1452.
[58] D. Qian, L. Ye, M. Zhang, Y. Liang, L. Li, Y. Huang, X. Guo, S. Zhang, Z.a. Tan, J. Hou, Macromolecules 45 (2012) 9611–9617.
[59] Z.-G. Zhang, B. Qi, Z. Jin, D. Chi, Z. Qi, Y. Li, J. Wang, Energy Environ. Sci. 7 (2014) 1966–1973.
[60] Y. Chen, X. Zhang, C. Zhan, J. Yao, ACS Appl. Mater. Interfaces 7 (2015) 6462–6471.
[61] A. Tang, C. Zhan, J. Yao, Adv. Energy Mater. 5 (2015) 1500059.
[62] D. Yan, W. Liu, J. Yao, C. Zhan, Adv. Energy Mater. 8 (2018) 1800204.

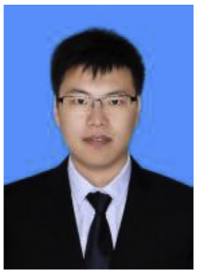

**Yuan Chang** received his Master degree from University of Chinese Academy of Sciences in 2018. He is currently a Ph.D. student under the supervision of Prof. He Yan at Hong Kong University of Science and Technology (HKUST), and a short-term visiting student supervised by Prof. Chuanlang Zhan at the Institute of Chemistry, Chinese Academy of Sciences (ICCAS) and College of Chemistry and Environmental Science, Inner Mongolia Normal University. His research currently focuses on fabrication of high efficiency organic solar cells.

**Xin Zhang** received his Ph.D. degree from Institute of Chemistry, Chinese Academy of Sciences under the supervision of Prof. Jiannian Yao and Prof. Chuanlang Zhan in 2015 and then worked as a Post Doctorate fellow with Prof. Chuanalng Zhan at ICCAS and with Prof. Xuefeng Guo at Peking University. Currently, his research focuses on synthesis of high-performance non-fullerene small molecule acceptors for organic solar cells.

**Yabing Tang** received his bachelor's degree in Materials Physical from Xi'an Jiaotong University in 2017. He joined Prof. Ma's group at Xi'an Jiaotong University as a master student of Prof. Yan in 2017. He is now working on the application of n-dopant in organic solar cells.

**Dr. Monika Gupta** was born in Allahabad city of Uttar Pradesh of India. She Graduated from Allahabad University with Bachelor's degree in Chemistry, Botany in 2006 then Master's degree in organic Chemistry in 2008. Later she lived in Mumbai to complete her Doctorate degree from Bhabha Atomic Research Centre. She was awarded with CAS PIFI fellowship in China and DST SERB NPDF fellowship in India in 2016 and worked as a Post Doctorate fellow with Prof. Chuanlang Zhan for two years at ICCAS in Beijing till 2018. Her research area includes synthesis of organic small molecules for Solar cells, fluorescent dye molecules, host-guest complexation and photochemistry.

**Miss Dan Su**, born in 1993, received her B.S. degree from China West Normal University in 2017. She is now a Master student at Hebei University supervised by Prof. Shuying Hou and a visiting student supervised by Prof. Chuanlang Zhan at ICCAS. Her research focuses on synthesis of organic photovoltaic materials.

**Jiaen Liang** obtained her B.S degree in pharmaceutical sciences from Wuhan University in 2018. She then joined Prof. Zhan's group as a short-term visiting student at ICCAS. She is currently a Ph.D. student under the supervision of Prof. He Yan at HKUST. Her research interests focus on the synthesis and application of organic photovoltaic materials.

**Dr. Dong Yan**, received her PhD in Chemistry from Institute of Chemistry, Chinese Academy of Sciences (CAS) in 2019, under the supervision of Prof. Jiannian Yao and Prof. Chuanlang Zhan. She received her Master degree in Materials Science at Institute of Physics and Chemistry, CAS, under the supervision of associate Prof. Yun Liu. Her research activities mainly focus on fabrications and structure-property relationship of organic solar cells.

**Kun Li**, born in 1995, received his B.S. degree from Henan Polytechnic University in 2017. He is now a Master student at Capital Normal University supervised by Prof. Hongbing Fu and a visiting student supervised by Prof. Chuanlang Zhan at ICCAS and College of Chemistry and Environmental Science, Inner Mongolia Normal University. His research focuses on the preparation and characterization of organic solar cells.

**Dr. Xuefeng Guo** received his Ph.D. in 2004 from the Institute of Chemistry, Chinese Academy of Sciences, Beijing. From 2004 to 2007, he was a postdoctoral research scientist at the Columbia University Nanocenter. He joined the faculty as a professor under “Peking 100-Talent” Program at Peking University in 2008. His current research is focused on functional nanometer/molecular devices.

**Prof. Dr. Wei Ma** obtained his Ph.D. in Chemical Physics from the University of Pierre Marie Curie (Paris 6, France) in 2010 before moving to the Ecole Normale Superieure (Paris), France (2010–1011) and North Carolina State University (NCSU) as Postdoc Fellow. He joined the School of Materials Science Engineering at Xi'an Jiaotong University in 2014 as a Professor. His research interests include the use of soft/hard X-ray based techniques to unravel the relationship between film microstructure and device performance.

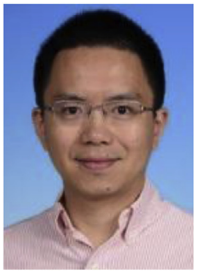

**Dr. He Yan** is Professor at Hong Kong University of Science and Technology (HKUST). After obtaining his doctor degree in 2004 at Northwestern University, Dr. Yan continued his research work at Polyera Corporation as a group leader and built up the organic solar cell research division of the company. In 2012, Dr. Yan returned to HKUST and continued his research on organic solar cells. In 2015, Dr. Yan's record efficiency cell was recorded in NREL chart. Dr. Yan is also one of first scholars reporting highly efficient non-fullerene organic solar cells with low voltage losses (*Nature Energy, 2016, 1, 16089*).

**Dr. Chuanlang Zhan** received his Ph. D. degree from Institute of Photographic Chemistry, Chinese Academy of Sciences (CAS), under supervision of Prof. Duoyuan Wang, and joined Institute of Chemistry, CAS, as a Postdoc fellowship at Laboratory of organic Solids, working with Prof. Daoben Zhu and Prof. Deqing Zhang. Later he was promoted as an associate professor at this institute. He is now a professor at ICCAS, working with Prof. Jiannian Yao, and a Professor at College of Chemistry and Environmental Science, Inner Mongolia Normal University. His research activities focus on synthesis and self-assembly of functional molecular materials, solar energy conversion, and solar cells.